

Review

Laser Cooling and Trapping of Rare-Earth-Doped Particles

Galina Nemova

Department of Electrical Engineering, Polytechnique Montréal, 2500 ch. de Polytechnique, Montréal, QC H3T 1H4, Canada; galina.nemova@videotron.ca

Abstract: This review focuses on optical refrigeration with the anti-Stokes fluorescence of rare-earth (RE)-doped low-phonon micro- and nanocrystals. Contrary to bulk samples, where the thermal energy is contained in internal vibrational modes (phonons), the thermal energy of nanoparticles is contained in both the translational motion and internal vibrational (phonons) modes of the sample. Much theoretical and experimental research is currently devoted to the laser cooling of nanoparticles. In the majority of the related work, only the translational energy of the particles has been suppressed. In this review, the latest achievements in hybrid optical refrigeration of RE-doped low-phonon micro- and nanoparticles are presented. Hybrid cooling permits the suppression of not only the translational energy of the RE-doped particles, but also their internal vibrational phonon thermal energy. Laser cooling of nanoparticles is not a simple task. Mie resonances can be used to enhance laser cooling with the anti-Stokes fluorescence of nanoparticles made of low-phonon RE-doped solids. Laser-cooled nanoparticles is a promising tool for fundamental quantum-mechanical studies, nonequilibrium thermodynamics, and precision measurements of forces.

Keywords: laser cooling of solids; rare-earth-doped materials; optical trapping; optical tweezers



Citation: Nemova, G. Laser Cooling and Trapping of Rare-Earth-Doped Particles. *Appl. Sci.* **2022**, *12*, 3777. <https://doi.org/10.3390/app12083777>

Academic Editor: Alessandro Belardini

Received: 8 March 2022

Accepted: 5 April 2022

Published: 8 April 2022

Publisher's Note: MDPI stays neutral with regard to jurisdictional claims in published maps and institutional affiliations.



Copyright: © 2022 by the author. Licensee MDPI, Basel, Switzerland. This article is an open access article distributed under the terms and conditions of the Creative Commons Attribution (CC BY) license (<https://creativecommons.org/licenses/by/4.0/>).

1. Introduction

Cooling or refrigeration is a physical process permitting the maintaining of a sample at a temperature below that of its surroundings. This technique dates back thousands of years to when people first tried to preserve food. The reliable source of coherent radiation (laser), demonstrated by Theodore Maiman in 1960, has revolutionized the cooling process. Laser cooling (optical refrigeration) and trapping have since been developed.

In late 1950 and the early 1960s, Wolfgang Paul and Hans Dehmelt introduced the first ion traps. Wolfgang Paul with colleagues developed the three-dimensional radiofrequency (RF) trap, known also as the Paul trap, from a linear quadrupole mass filter. It can be considered as a two-dimensional ion trap [1]. Hans Dehmelt and a number of groups working independently proposed a magnetic field for trapping [2–7]. Dehmelt named this trap the Penning trap after Frans Penning who, in 1936, proposed the use of a magnetic field to an electrical discharge in order to increase the lifetime of electrons using the confining effect of the field [7].

In 1968, Vladilen Letokhov proposed the use of the dipole force to trap atoms [8]. The electric dipole interaction between the atoms and a standing laser wave was used to form a periodic lattice of potential wells. In this lattice, minima coincided with the nodes or antinodes of the standing laser wave.

In 1975, Doppler cooling was proposed by two teams: Theodor Hansch and Arthur Leonard Schawlow for free atoms [9], and David Wineland and Hans Georg Dehmelt for trapped particles [10]. Doppler cooling occurs when atoms are irradiated with counter-propagating laser beams detuned below resonance. Following the Doppler mechanism, a moving atom absorbs photons into the laser wave counterpropagating its velocity rather than into the copropagating wave; thus, it encounters a force opposed to its velocity and undergoes cooling.

In 1988, it was realized that, using multilevel atoms and the spatial variation of light polarization, a temperature lower than the Doppler cooling limit can be achieved [11]. This technique is known as sub-Doppler, polarization gradient, or Sisyphus cooling.

In 1995, a fifth, low-energy form of matter (Bose–Einstein condensate) was demonstrated by Eric Cornell and Carl Wieman in a gas of rubidium atoms, which was cooled to 170 nK, [12] and by Wolfgang Ketterle in a gas of sodium atoms [13].

All these developed techniques cause laser cooling of the center-of-mass motion of atoms, ions, or particles. Indeed, the energy of molecules in gases almost completely belong to translational degrees of freedom. Using one of the mentioned methods, the translational temperature of a nanocrystal can be decreased. This process is known as translational cooling. In 1929, Peter Pringsheim proposed the use of anti-Stokes fluorescence for cooling [14]. Following this approach, the internal energy included in the crystal lattice vibrations can be removed from a number of solids. Laser trapping and cooling rare-earth (RE)-doped particles are considered in this review. The theory of laser cooling with anti-Stokes fluorescence is briefly discussed in Section 2. Recent achievements in the development of optical trapping and cooling of micro- and nanoparticles are presented in Section 3.

2. Laser Cooling of Bulk Rare-Earth-Doped Solids

In the majority of cases, a luminescent material interacting with light emits photons with a lower energy compared to the energy of the absorbed photons (Figure 1a). This effect is called the Stokes shift. The law of conservation of energy applied to these redshifted emitted photons explains heating of the optical material caused by phonon generation (Figure 1a). If the energy of the emitted photons exceeds the energy of absorbed ones, the anti-Stokes shift, accompanied by phonon absorption, takes place in the system (Figure 1b).

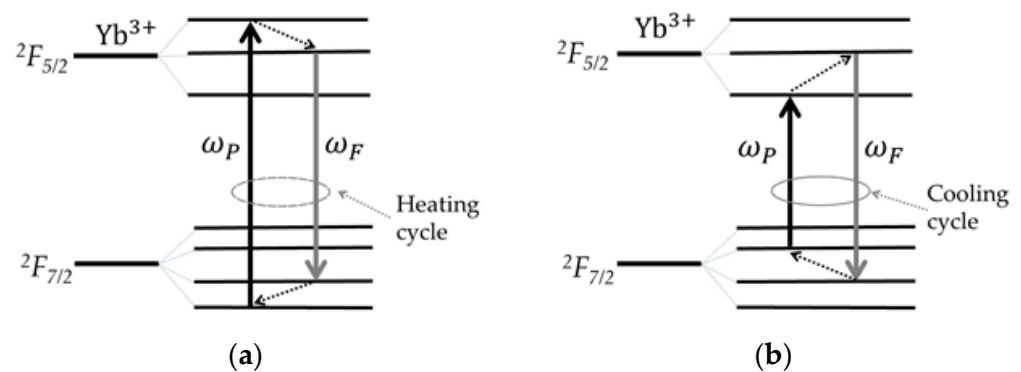


Figure 1. Energy levels of Yb^{3+} ions doped in a solid. Arrows illustrate the excitation and decay processes for (a) Stokes and (b) anti-Stokes cycles.

As mentioned above, in 1929, Pringsheim proposed the use of anti-Stokes fluorescence for optical refrigeration [14]. In 1995, laser cooling with anti-Stokes fluorescence was reached for RE-doped solids [15]. In this first proof-of-principle experiment, an ytterbium (Yb^{3+})-doped fluorozirconate $\text{ZrF}_4\text{-BaF}_2\text{-LaF}_3\text{-AlF}_3\text{-NaF-PbF}_2$ (ZBLANP) sample was cooled down to only 0.3 K below the environmental temperature.

Let us consider in detail a laser cooling cycle in a Yb^{3+} -doped sample. As one can see in Figure 2, it includes photon absorption at the frequency ν_P , electron thermalization in the excited $^2F_{5/2}$ manifold accompanied by phonon absorption, and spontaneous photon emission from the excited $^2F_{5/2}$ manifold to the ground $^2F_{7/2}$ manifold.

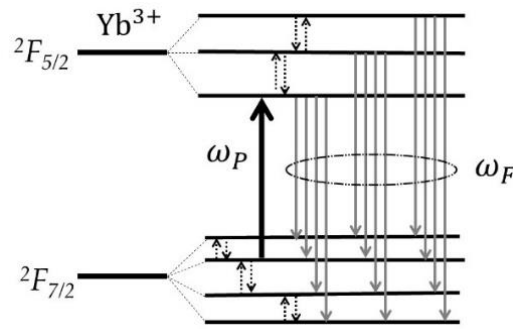


Figure 2. Energy levels of Yb³⁺ ions doped in a solid. Arrows illustrate the excitation and decay processes for a cooling cycle.

All photon absorption–emission cycles where the energy of the radiated photon exceeds the energy of the absorbed one (anti-Stokes fluorescence) result in cooling, as this energy difference has to be compensated by phonon absorption (Figure 2). All the photon absorption–emission cycles where the energy of the absorbed photons exceeds the energy of the radiated ones (Stokes fluorescence) causes heat generation photons in the sample, as the energy difference in these cycles has to be compensated by phonon generation (Figure 2). Spontaneous emission is characterized by the mean fluorescence frequency,

$$\nu_F = \frac{\int \Phi(\nu)\nu d\nu}{\int \Phi(\nu)d\nu} \tag{1}$$

where $\Phi(\nu)$ is the fluorescence flux density, which can be obtained experimentally, and $\nu_F = c/\lambda_F$. Here, λ_F is the mean fluorescence wavelength and c is the speed of light in vacuum. If one wants to cool a sample, the pump frequency, ν_P , is bound to be smaller than the mean fluorescence frequency, ν_F , and all radiated anti-Stokes photons must leave the sample (not to be reabsorbed by Yb³⁺ ions). Indeed, these anti-Stokes reabsorbed photons serve as the source of heat generation in the sample, which is undesirable for cooling. The efficiency of the cooling cycle is the difference between the energy of the anti-Stokes emitted photon and the energy of the pump photon normalized by the energy of the pump photon that is

$$\eta_{cool} = \frac{h\nu_F - h\nu_P}{h\nu_P} = \frac{\lambda_P}{\lambda_F} - 1. \tag{2}$$

The electrons excited to the 2F_{5/2} manifold can also decay nonradiatively to the ground 2F_{7/2} manifold, generating phonons. The “competition” between the radiative and nonradiative decays of the 2F_{5/2} electrons can be quantified by the quantum efficiency,

$$\eta_q = \frac{W_r}{W_r + W_{nr}} \tag{3}$$

where $W_r = 1/\tau_r$ and $W_{nr} = 1/\tau_{nr}$ are the radiative and nonradiative decay rates, respectively, with τ_r and τ_{nr} being the radiative and nonradiative lifetimes of the excited manifold, respectively. If the quantum efficiency of the anti-Stokes generation process is very high ($\eta_q \geq 99\%$), laser cooling caused by the removal of phonon energy with anti-Stoke photons from the material takes place in the system, as the probability of nonradiative decay with phonon generation from the excited 2F_{5/2} to the ground 2F_{7/2} manifold is very low [16]. Only such samples are suitable for laser cooling.

To simulate cooling in a RE-doped sample, one can use a two-level model developed in [17,18]:

$$\begin{cases} \frac{dN_1}{dt} = \frac{I_p}{h\nu_p} [N_0\sigma_a(\nu_p) - N_1\sigma_e(\nu_p)] - \frac{N_1}{\tau_r} - \frac{N_1}{\tau_{nr}} \\ N_T = N_0 + N_1 \end{cases} \tag{4}$$

where N_T is the RE ions density in the sample, and N_0 and N_1 are the population density in the ground and excited manifolds, respectively. I_p is the pump intensity at the frequency ν_p . $\sigma_{a,e}(\nu_p)$ is the absorption (a) and emission (e) cross-sections at the pump frequency ν_p . The cooling power density generated in the sample, P_{cool} , is the difference between the absorbed power density and radiated power density.

$$P_{cool} = -I_p [N_0\sigma_a(\nu_p) - N_1\sigma_e(\nu_p)] + N_1 \frac{h\nu_f}{\tau_r} - N_1 \frac{h\nu_f}{\tau_{nr}} \tag{5}$$

The cooling power generated in a sample of volume V when the system is in the steady-state regime ($dN_1/dt = 0$) is [19]

$$P_{cool}^V = \frac{h\tilde{\nu}_F - h\nu_P}{h\nu_P} \frac{VN_T\sigma_a(\nu_P)I_P}{\left[1 + \frac{I_P}{I_S} \left(1 + \frac{\sigma_e(\nu_P)}{\sigma_a(\nu_P)}\right)\right]} \approx \frac{h\tilde{\nu}_F - h\nu_P}{h\nu_P} VN_T\sigma_a(\nu_P)I_P \tag{6}$$

where $I_S = h\nu_P / [\eta_q\tau_r\sigma_a(\nu_P)]$ is the saturation intensity and $\tilde{\nu}_F = (2\eta_q - 1)\nu_F \approx \eta_q\nu_F$ is the effective mean fluorescence frequency. If the sample is placed on a low-contact and low-thermal conductivity support in a vacuum chamber, only radiative heat load may take place in the system. The final equilibrium temperature of the sample, T_S , can be estimated by the Stefan–Boltzmann law,

$$P_{cool}^V = \varepsilon\sigma_B S (T_r^4 - T_S^4) \tag{7}$$

where S is the total surface area of the sample, T_r is room temperature, and ε is the sample emissivity.

Since the first experimental observation in 1995, laser cooling of solids has been realized with Yb^{+3} , Er^{+3} , Tm^{+3} , and Ho^{+3} ions doped in a wide variety of low-phonon glasses and crystals including ZBLAN (maximum phonon energy of 580 cm^{-1}), ZBLANP (505 cm^{-1}), CBNZn (370 cm^{-1}), YAG (630 cm^{-1}), BYF (450 cm^{-1}), YLF (350 cm^{-1}), KPC (203 cm^{-1}), and LLF (420 cm^{-1}) [16,19–26]. Yb^{+3} ions are the most suitable RE ions for laser cooling application. Yb^{+3} ions have only one excited manifold. They are free from excited-state absorption, a source of undesirable nonradiative decay resulting in heat generation.

The resonant absorption coefficient, $\alpha_r(\nu, T)$, can be estimated as a product of the absorption cross-section $\sigma_a(\nu, T)$ and the thermal population density, $N_0(E_{0i}, T)$, of the initial state with the energy E_{0i} that is $\alpha_r(\nu, T) = \sigma_a(\nu, T) \cdot N_0(E_{0i}, T)$. Following the Boltzmann distribution, the thermal population density of the initial state is $N_0(E_{0i}, T) \sim \exp(-E_{0i}/\kappa_B T)$. The absorption cross-section is proportional to the Voigt spectral line $\sigma_a(\nu, T) \sim g_\nu(\nu, T)$, which is a result of the convolution of two broadening mechanisms: one that causes a Gaussian broadening and the other that produces a Lorentzian profile. Consequently, the resonant absorption coefficient can be presented as

$$\alpha_r(\nu, T) \sim g_\nu(\nu, T) \cdot \exp(-E_{0i}/\kappa_B T) \tag{8}$$

The inhomogeneous broadening is dominant for glass hosts as a result of structural disorder in glasses. It almost does not change with temperature, that is, $g_\nu(\nu, T)$ is almost constant and

$$\alpha_r(\nu, T) \sim \exp(-E_{0i}/\kappa_B T) \tag{9}$$

In glasses, the peak absorption coefficient α_r decreases exponentially with temperature. In crystal hosts, homogeneous broadening is dominant. The homogeneous linewidth scales as $\sim T^2$ and is associated with the two-phonon Raman scattering in the temperature range of 40–300 K. The peak absorption coefficient is proportional to

$$\alpha_r \sim T^{-2} \cdot \exp(-E_{0i}/\kappa_B T) \tag{10}$$

As one can see in relations (9) and (10), when the temperature decreases, the peak absorption coefficient α_r in crystals is higher than in glasses. Crystal hosts are the best choice for laser cooling.

Today’s record temperature of optical refrigeration is 93 ± 1 K. It was reached with a 10% $\text{Yb}^{3+}:\text{YLF}$ sample [25].

3. Optical Refrigeration of Rare-Earth-Doped Particles

In the majority of cases, bulk, $cm-$ and $mm-$ sized RE-doped low-phonon samples were laser-cooled. Optical refrigeration of RE-doped samples with different shapes and sizes was investigated in [27].

Three different approaches can be used to calculate the optical force applied to a particle. These approaches depend on the size of the particles compared to the wavelength of the laser beam. If the radius r of the particle is much larger than the light wavelength λ ($r > 20\lambda$), diffractive effects can be neglected. In this case, geometrical optics (ray optics) can be used for the optical force calculation. If the particle radius is comparable to the light wavelength ($r \sim \lambda$), the wave’s scattering should be considered. If the particle radius is much smaller than the light wavelength ($r \ll \lambda$), dipole approximation can be used.

3.1. Laser Cooling of Rare-Earth-Doped Mie Resonant Samples

In 1908, Gustav Mie developed the theory of the plane-wave scattering by spheres of arbitrary size (Mie theory) [28]. Following Mie theory, a sphere can support eigenmodes (the Mie resonant modes) if the radius of the sphere and the pump wavelength are properly arranged. Different eigenmodes have different electric field intensity distributions inside the sphere. As noted above, if a sphere radius is much smaller than the wavelength of the incident light ($r \ll \lambda$), the responses of the sphere to the incident light can be represented by an electric dipole and a magnetic dipole (the Rayleigh or dipole approximation). According to Mie theory, the pump plane wave can be expanded in spherical harmonics as

$$\vec{E}_P = E_0 \sum_{n=1}^{\infty} i^n \frac{2n+1}{n(n+1)} [M_{o1n}^{(1)} - iN_{e1n}^{(1)}] \tag{11}$$

where E_0 is the amplitude of the incident field, and $M_{o1n}^{(1)}$ and $N_{e1n}^{(1)}$ are the vector spherical harmonics,

$$M_{o1n}^{(1)} = \cos\varphi \cdot \pi_n(\cos\theta) \cdot j_n(\tilde{r})\hat{e}_\theta - \sin\varphi \cdot \tau_n(\cos\theta)j_n(\tilde{r})\hat{e}_\varphi \tag{12}$$

$$N_{e1n}^{(1)} = n(n+1) \cos\varphi \cdot \sin\theta \cdot \pi_n(\cos\theta) \cdot \frac{j_n(\tilde{r})}{\tilde{r}}\hat{e}_r + \cos\varphi \cdot \tau_n(\cos\theta) \frac{[\tilde{r}j_n(\tilde{r})]'}{\tilde{r}}\hat{e}_\theta - \sin\varphi \cdot \pi_n(\cos\theta) \frac{[\tilde{r}j_n(\tilde{r})]'}{\tilde{r}}\hat{e}_\varphi \tag{13}$$

where $\tilde{r} = 2\pi n_{\text{Yb}} r / \lambda_P$ and r is the radial distance. The index $n = 1$ stands for dipole, $n = 2$ for quadrupole, etc., j_n are the spherical Bessel functions, and π_n and τ_n are the angle-dependent functions defined as

$$\pi_n = \frac{P_n^1}{\sin\theta} \tag{14}$$

and

$$\tau_n = \frac{dP_n^1}{d\theta} \tag{15}$$

where P_n^1 is the associated Legendre function of the first kind of degree n and the first order. The field inside the sphere is

$$\vec{E} = E_0 \sum_{n=1}^{\infty} i^n \frac{2n+1}{n(n+1)} [c_n M_{o1n}^{(1)} - id_n N_{e1n}^{(1)}] \tag{16}$$

where the coefficients c_n and d_n are functions of the normalized radius of the sphere, $x = 2\pi R/\lambda_P$, with R being the radius of the sphere, and

$$c_n = \frac{j_n(x) [xh_n^{(1)}(x)]' - h_n^{(1)}(x) [xj_n(x)]'}{j_n(mx) [xh_n^{(1)}(x)]' - h_n^{(1)}(x) [mxj_n(mx)]'} \tag{17}$$

$$d_n = \frac{mj_n(x) [xh_n^{(1)}(x)]' - mh_n^{(1)}(x) [xj_n(x)]'}{m^2j_n(mx) [xh_n^{(1)}(x)]' - h_n^{(1)}(x) [mxj_n(mx)]'} \tag{18}$$

where $h_n^{(1)}$ is the spherical Hankel functions, $m = n_{Yb}$. The c_n coefficients correspond to the magnetic multipole modes and the d_n coefficients correspond to the electric multipole modes. If, for some values of R , the denominator of coefficient c_n or the denominator of d_n vanishes, the sphere resonates and scatters, exhibiting a peak. The radial distribution of the absolute-square of the electric field averaged over the polar angle, θ , and azimuthal angle, φ , of spherical coordinates looks like

$$\langle |\vec{E}|^2 \rangle = \frac{E_0^2}{4} \sum_{n=1}^{\infty} (m_n |c_n|^2 + n_n |d_n|^2) \tag{19}$$

where m_n and n_n are functions of the radial distance, r , and are given as

$$m_n = 2(2n + 1) |j_n(\tilde{r})|^2 \tag{20}$$

$$n_n = 2n(2n + 1) \left[(n + 1) \left| \frac{j_n(\tilde{r})}{\tilde{r}} \right|^2 + \left| \frac{(\tilde{r} \cdot j_n(\tilde{r}))'}{\tilde{r}} \right|^2 \right] \tag{21}$$

where $\tilde{r} = 2\pi n_{Yb} r / \lambda_P$.

The cooling power generated in the sphere can be calculated as the difference between the pump power absorbed by the Yb^{3+} ions in the sphere and the power radiated with anti-Stokes fluorescence at the mean fluorescence wavelength. The field intensity given by relation (19) can then be integrated over the nanosphere and then inserted into relation (6) as

$$P_{cool}^V = 4\pi \left(\frac{h\tilde{\nu}_F - h\nu_P}{h\nu_P} \right) N_T \sigma_a(\nu_P) \sqrt{\frac{\epsilon_0}{\mu_0}} \int_0^R \langle |\vec{E}|^2 \rangle r^2 dr, \tag{22}$$

which corresponds to the cooling power generated in the Mie-resonant nanosphere.

Laser cooling of RE-doped low-phonon microparticles enhanced with Mie resonant modes was considered in [29]. By way of example, an Yb^{3+} :YAG nanosphere pumped with the plane electromagnetic wave propagating in vacuum at the pump wavelength $\lambda_P = 1030$ nm located in the long wavelength tail of the Yb^{3+} absorption spectrum was considered (Figure 3). The mean fluorescence wavelength of the spontaneous radiation $\lambda_F < \lambda_P$. A bulk Yb^{3+} :YAG sample was laser-cooled in [26].

A sample with an Yb^{3+} ion concentration of ~10% was investigated in [29]. This concentration is smaller than the critical concentration of Yb^{3+} :YAG (17%). Such samples are free from cooperative effects such as resonant-radiative transfer (reabsorption) and resonant nonradiative transfer, which deteriorate laser cooling [19]. Indeed, these cooperative effects result in the excited energy migration from the ion to ion inside the sample. This migrating energy can excite impurities in the sample and decay nonradiatively, causing heat generation in the sample. The pump power considered in [29] was $I_P = 0.5 \cdot 10^{-4}$ W/ μm^2 . The cooling power density generated in the nanosphere is equal to

$$\rho_{cool} = P_{cool}^V / V \tag{23}$$

where $V = \frac{4}{3}\pi R^3$ is the volume of the sphere. R is the radius of the sphere. The cooling power density, ρ_{cool} , for nanospheres with different radii in the range between 150 nm and 650 nm was estimated using relations (22) and (23). The results are plotted in Figure 4. It changes considerably on this range and has several peaks. The radii of the nanospheres corresponding to these peaks are very close to the resonant radii of the Mie resonant modes including the magnetic dipole (MD) modes, the magnetic quadrupole (MQ) modes, the electric dipole (ED) modes, and the electric quadrupole (EQ) modes.

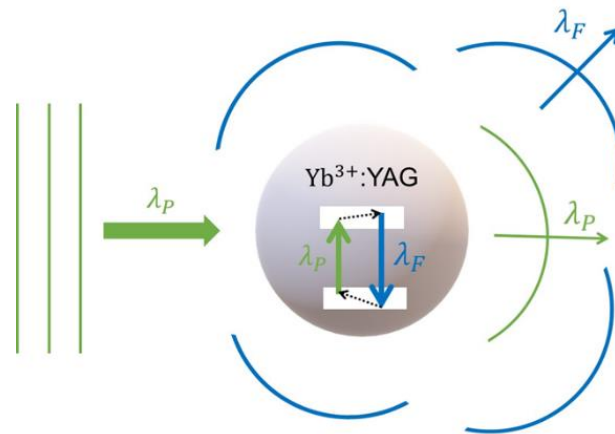


Figure 3. System under investigation. Here, λ_P and λ_F are the pump and mean fluorescence wavelengths, respectively [29].

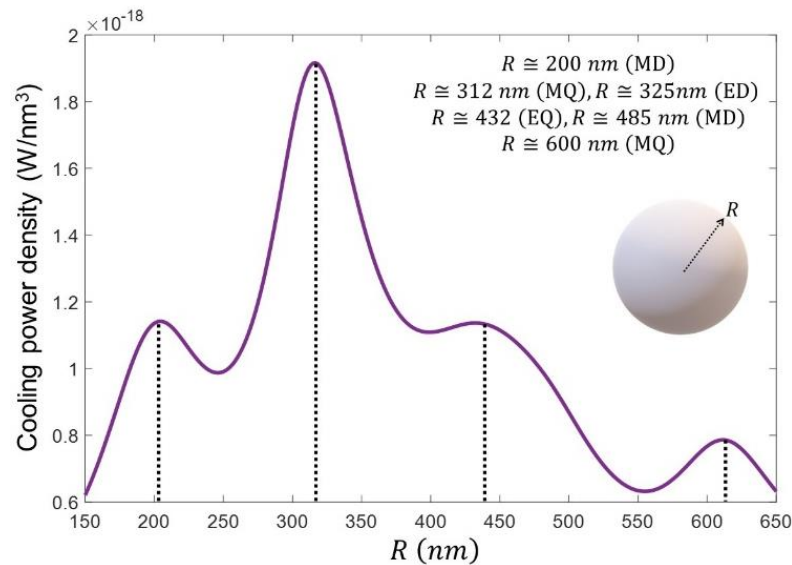


Figure 4. Cooling power density generated in nanospheres with different radii. Resonant radii of the nanospheres supporting MD, ED, MQ, and EQ modes are presented for simplicity of understanding [29].

With the knowledge of the cooling power density, ρ_{cool} , it is possible to estimate the temperature of the nanospheres placed on a low-contact and low-thermal-conductivity support in a vacuum chamber, using Equation (7). These results are presented in Figure 5. As one might expect, the radii of the nanospheres for which the temperature reaches minima almost perfectly coincide with those associated with the highest cooling power density (Figure 4).

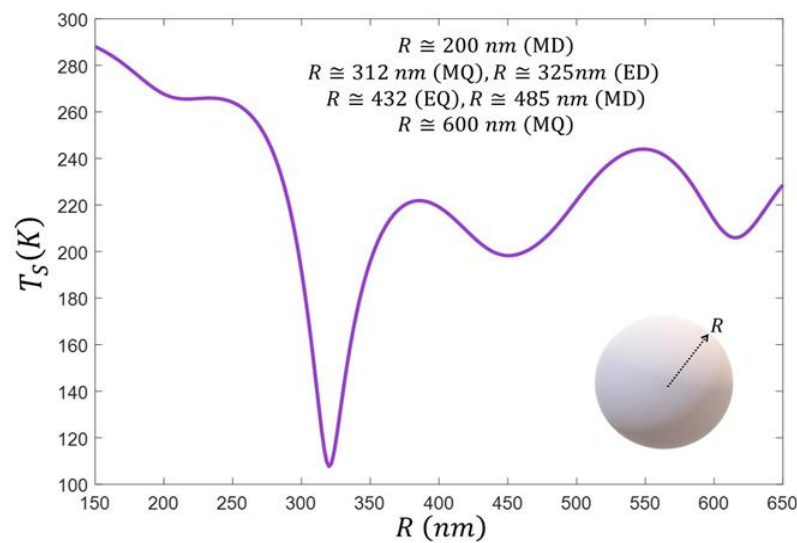


Figure 5. Sample temperature, T_s , versus the radius of the sample. Resonant radii of the nanospheres supporting MD, ED, MQ, and EQ modes are presented for simplicity of understanding [29].

In [30], a nanoscale semiconductor optomechanical resonator (CdSNR) was laser-cooled with a Yb^{3+} :YLF microcrystal attached to it. The Yb^{3+} :YLF microcrystal was hydrothermally synthesized. The cooling process with a microscopic cooler provided local cooling. This approach permits a thermal steady temperature state for nanoscale devices to be achieved. A CdSNR was placed at the end of a silicon substrate. A 10% Yb^{3+} :YLF crystal was placed at the free end of the CdSNR cantilever. The 10% Yb^{3+} :YLF crystal was hydrothermally grown. The silicon substrate was located inside a cryostat chamber, which was pumped to $\sim 10^{-4}$ torr (Figure 6).

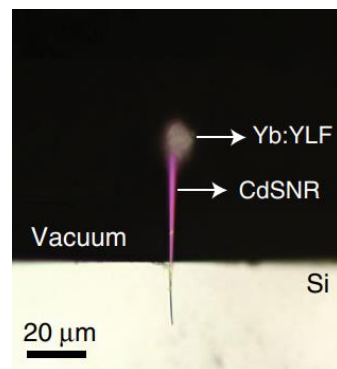


Figure 6. The CdSNR cantilever supported by a silicon substrate. A Yb^{3+} :YLF crystal is placed at the free end of the cantilever [30].

The temperature of the Yb^{3+} :YLF placed at the end of the cantilever was measured with differential luminescence thermometry (DLT) [31,32]. Emission from different crystal-field levels of Yb^{3+} ions was analyzed using a Boltzmann distribution. At an incident power $P_0 = 40.1 \text{ mW}$ and spot radius $w_0 = 1.15 \text{ μm}$, a temperature drop of 23.6 K below room temperature was observed.

A cantilever of length L , width W , and thickness H was considered for computer simulations. The Yb^{3+} :YLF crystal of $H_{\text{YLF}} = 6 \text{ μm}$, $L_{\text{YLF}} = 7.5 \text{ μm}$, and $W_{\text{YLF}} = 6 \text{ μm}$ was approximated as a cuboid. The volume and aspect ratio were almost the same as for the crystal used in experiments (Figure 7). The thermal conductivity of the YLF crystal ($\sim 6 \text{ Wm}^{-1}\text{K}^{-1}$) was relatively large. It resulted in an almost uniform temperature distribution in the crystal.

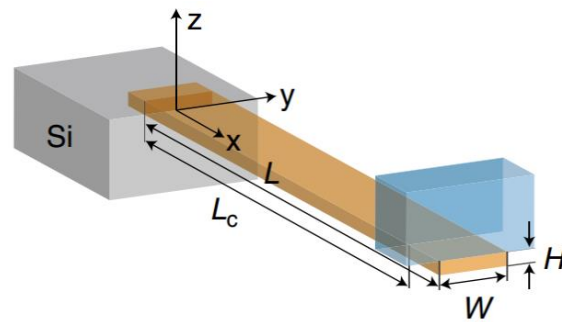


Figure 7. The geometry of the system [30].

As the cantilever was placed in the vacuum chamber, conduction and convection were absent. The temperature at the silicon/CdS interface ($x = 0$) was equal to the cryostat temperature. The authors of the paper assumed that all of the heat generated in the Yb^{3+} :YLF crystal was transferred to or from the CdSNR across the interface at $x = L_c$. They calculated a cooling power for the sample with $H = 150 \text{ nm}$, $W = 2.5 \text{ }\mu\text{m}$, and $L_c = 53 \text{ }\mu\text{m}$ and estimated that the coldest point in the cantilever was between 26 K and 58 K below room temperature. The calculated cooling power was smaller than the experimentally obtained cooling power. The discrepancy can be explained in the following way: the size of the YLF microcrystals corresponds to the Mie scattering regime. Internal optical fields may be enhanced considerably by cavity resonances.

In 2021, 10% Yb^{3+} -doped LiLuF_4 (LLF) microcrystals were grown with a hydrothermal process [33]. They were transferred to electron-transparent Si_3N_4 windows irradiated by a near-infrared laser for solid-state laser refrigeration of windows in vacuum (10^{-3} torr) (Figure 8).

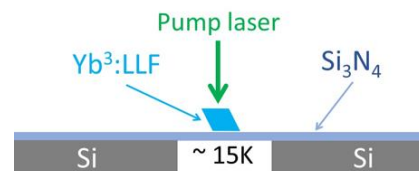


Figure 8. Schematic of 10% Yb^{3+} :LLF microcrystals placed on a Si_3N_4 TEM window.

Analysis of the Yb^{3+} luminescence spectrum at an irradiance of 0.854 MWcm^{-2} revealed laser cooling by more than 20.4 K below room temperature. Using computer simulations, bulk cooling of the Si_3N_4 window by $\sim 15 \text{ K}$ was demonstrated. The silicon substrate was at room temperature. In 2022, 10% Yb^{3+} : LiLuF_4 (Yb^{3+} :LLF) crystals synthesized using a safe and scalable hydrothermal method were laser-cooled more than 15 K below room temperature in air and 5 K in deionized water. They were pumped with a 1020 nm diode laser [34].

3.2. Laser Trapping and Cooling Rare-Earth-Doped Particles

Consider RE-doped particles under both translational and internal laser cooling. Currently available methods for nanoparticle cooling allow translational temperatures of a few hundred microkelvin to be achieved [35]. Consider new mechanisms of optical cooling that allow us to reduce the translational temperature of a sample concurrently with its internal cooling, which tends to decrease the internal temperature of the sample.

Here, 10% Yb^{3+} -doped $\beta\text{-NaYF}_4$ nanowires in a fluid medium (D_2O) were laser-trapped and cooled with a near-infrared single-beam at the wavelength 1020 nm (inset in Figure 9) [36]. $\beta\text{-NaYF}_4$ nanowires were prepared using a low-cost, scalable hydrothermal synthesis [37]. A nanowire can be considered as a cylinder (height $\sim 2000 \text{ nm}$) with a hexagonal cross-section (edge $\sim 255 \text{ nm}$). As one can see in Figure 9a, undoped (0% Yb^{3+}) $\beta\text{-NaYF}_4$ nanowires under identical conditions (an irradiance of 73 MWcm^{-2} at the pump wavelength 1020 nm) undergo heating by $6 \text{ }^\circ\text{C}$ above the ambient temperature.

At an irradiance of 73 MWcm^{-2} , nanowires were observed to refrigerate by $> 9^\circ\text{C}$ below ambient temperature (Figure 9b).

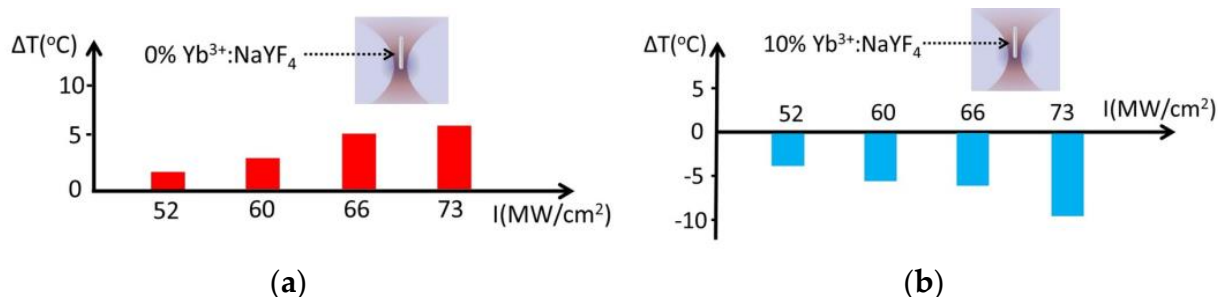


Figure 9. Temperature of individually trapped $\beta\text{-NaYF}_4$ nanowires under 1020 nm laser irradiance: (a) undoped samples (0% $\text{Yb}^{3+}:\text{NaYF}_4$) and (b) 10% $\text{Yb}^{3+}:\text{NaYF}_4$ samples.

In [38], a similar approach based on single-beam laser trapping at the wavelength 1020 nm was used for optical refrigeration of $\text{Yb}^{3+}:\text{YLF}$ nanocrystals (Figure 10a) prepared using the same method as in [36]: low-cost, scalable hydrothermal synthesis [37]. Using cold Brownian motion analysis, the temperature of an $\text{Yb}^{3+}:\text{YLF}$ nanocrystal in a fluid medium (D_2O) was estimated for different irradiances (Figure 10b).

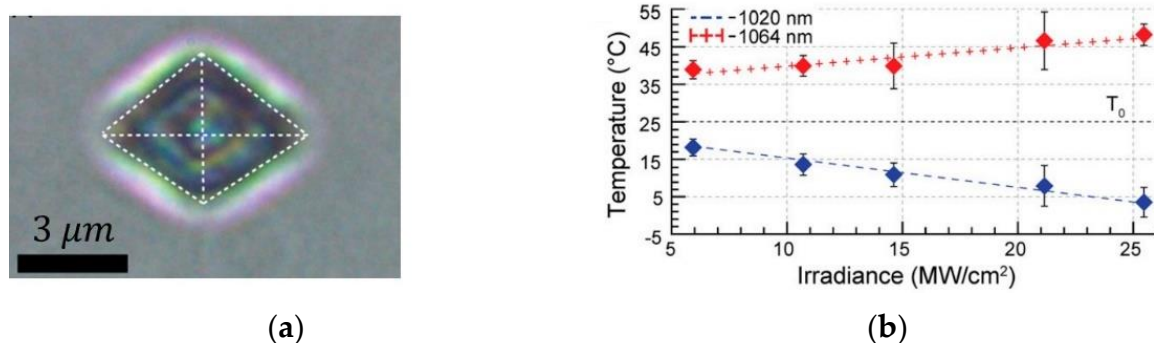


Figure 10. Laser cooling of laser-trapped $\text{Yb}^{3+}:\text{YLF}$ microcrystals. (a) Optical micrograph of a laser-trapped $\text{Yb}^{3+}:\text{YLF}$ crystal. (b) Temperature of laser-trapped particles in D_2O as determined using the cold Brownian motion analysis [38].

As one can see in Figure 10b, trapping at the wavelength 1064 nm gives rise to heating of a sample. The wavelength $\lambda_p = 1064 \text{ nm}$ is energetically insufficient to be absorbed by Yb^{3+} ions and subsequently cannot initiate upconversion laser cooling. At the trapping wavelength of 1020 nm, 10% $\text{Yb}^{3+}:\text{YLF}$ crystals were observed to cool from 19°C at a 5.9 MWcm^{-2} trapping irradiance to 4°C at a 25.5 MWcm^{-2} trapping irradiance (Figure 10b).

In the cases being considered, laser refrigeration of RE-doped particles has been demonstrated in optical tweezers in liquid. It was analyzed by measuring cold Brownian motion. Consider optical refrigeration of RE-doped levitated particles optically trapped in a low-pressure environment. The ability to arrange levitated particles in vacuum is a promising instrument for understanding macroscopic quantum mechanics [32].

The changes in fluorescence of the nanocrystal as a function of laser trap wavelength were used to measure the temperature of the particle. Indeed, fluorescence spectra are directly related to the relative populations of sublevels of the excited $^2F_{5/2}$ manifold via the Boltzmann distribution. The changes in the damping of the motion of the nanocrystal with the temperature were also used for temperature measurements.

When the optically refrigerated particle is levitated in gas, cooling of the gas molecules surrounding the particle takes place in the system. A modification in the local gas viscosity

also takes place in the system. The damping rate of the translational motion of a particle undergoes changes as a result of hot or cold Brownian motion of the particle. The effect was used to measure particle temperature. Figure 11 shows the temperatures of 13 particles trapped using laser light at 1031 nm and 1064 nm at a pressure of 600 mbar. The trapping power was 200 mW. Some changes between the temperatures of particles trapped by 1031 nm light was observed. The average internal temperature was ~ 167 K. The lowest temperature reached in this experiment was ~ 130 K. As one can see in Figure 11, in the beginning of the experiment, particle 2 was trapped using a 1031 nm laser beam. The temperature reached was 175 K. Later, the laser wavelength was changed to 1064 nm. For this wavelength, the temperature reached was 255 K (Figure 11). For this particle, the temperature was 175 K when trapped with 1031 nm light and 255 K when trapped using 1064 nm light (Figure 11). Using (6) and (7), one can show that lower temperatures can be achieved with a laser at 1020 nm. Lower pressure and improved crystal purity can also help to reach lower temperatures.

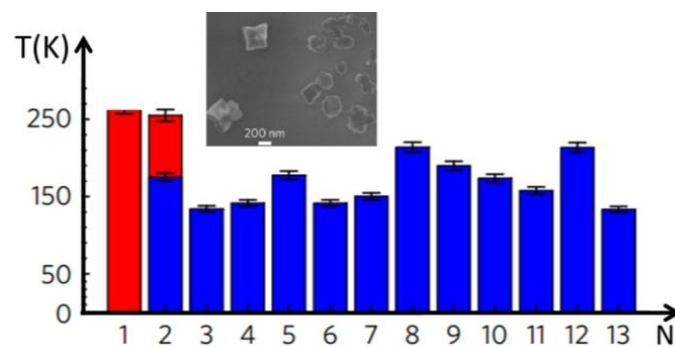


Figure 11. $\text{Yb}^{3+}:\text{YLF}$ crystals (inset) and their internal temperatures for 1031 nm (red) and 1064 nm (blue) trapping wavelengths. N is the particle number.

Anti-Stokes cooling of $\text{Yb}^{3+}:\text{NaYF}$ nanocrystals was reported in [39]. A sublevel splitting of Yb^{3+} ions doped in a NaYF host is smaller than that of Yb^{3+} ions doped in other crystal hosts. $\text{Yb}^{3+}:\text{NaYF}$ can provide better cooling efficiency. $\text{Yb}^{3+}:\text{NaYF}$ particles appeared as spheres (insert in Figure 12). The fabrication process of $\text{Yb}^{3+}:\text{NaYF}$ nanoparticles is safer than the fabrication process of $\text{Yb}^{3+}:\text{YLF}$ nanoparticles. It is predicted that $\text{Yb}^{3+}:\text{NaYF}$ can be cooled to ~ 5 K colder than $\text{Yb}^{3+}:\text{YLF}$ crystals [38]. In 2021, 10% $\text{Yb}^{3+}:\text{NaLF}_4$ optically levitated nanoparticles were laser-cooled by 42 K to a temperature of 252 K [39]. The ytterbium ions were excited with a laser at 1020 nm.

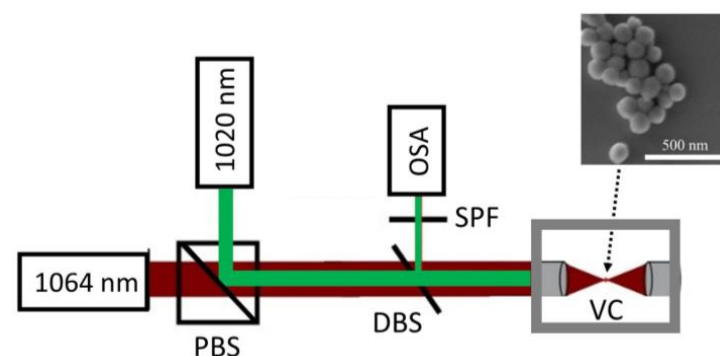


Figure 12. Laser trapping and cooling $\text{Yb}^{3+}:\text{NaYF}$ nanocrystals. A 1064 nm laser was used for the optical-dipole-trapping of $\text{Yb}^{3+}:\text{NaYF}$ nanocrystals in a vacuum chamber. A 1020 nm laser was used for anti-Stokes laser-cooling of $\text{Yb}^{3+}:\text{NaYF}$ nanocrystals. PBS: Polarizing Beam Splitter, DBS: Dichroic Beam Splitter, SPF: Short-Pass Filter, OSA: Optical Spectrum Analyzer.

A 1064 nm laser was used to create an optical dipole trap. A 1064 nm laser induced a dipole in the $\text{Yb}^{3+}:\text{NaYF}$ nanocrystal. The induced dipole moved to the point of highest

intensity of the laser field. The beam of a 1020 nm laser was collinear to the beam of the 1064 nm laser. The 1020 nm laser was responsible for anti-Stokes cooling in the system.

As one can see in Figure 12, anti-Stokes photoluminescence (PL) of the trapped crystal was collected with the lens used to focus the trapping and cooling laser beams. A 1000 nm dichroic beam splitter and a 1000 nm short-pass filter permitted the separation of the PL from the laser light. The filter cut-off PL at wavelengths higher than 1000 nm (Figure 12). The collected PL was analyzed with an OSA. These spectra were used to estimate the temperature of the sample. The lowest temperatures reached by seven nanocrystals are presented in Figure 13.

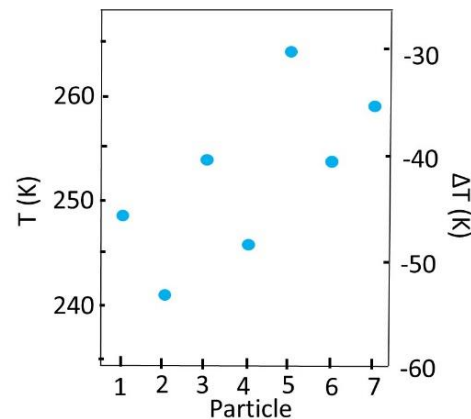


Figure 13. The lowest temperatures of seven nanocrystals (left axis). The decreases in the crystal's temperature reached by seven nanocrystals (right axis).

The decrease in the crystal's temperature was $\Delta = 42$ K. The lowest temperature reached was 252 K. The best decrease in the crystal's temperature $\Delta = 53$ K and the best lowest crystal's temperature 241 K were reached with one of the crystals (crystal 2).

In 2021, laser cooling of 8.6 ± 2.1 K below room temperature was observed with 10% Yb^{3+} :KLuF₄ microcrystals synthesized with hydrothermal methods [40]. The experimental results achieved in laser cooling of RE-doped nanoparticles are presented in Table 1.

Table 1. Reported results in optical refrigeration of nanoparticles. ΔT (K) is the temperature drop.

Sample	Pump Wavelength (nm)	ΔT (K)	Reference
Yb^{3+} :YLF	1020	23.6 (vacuum)	[30]
Yb^{3+} :YLF	1020	19 (D ₂ O)	[38]
Yb^{3+} :YLF	1031	126 (vacuum)	[32]
Yb^{3+} :LLF	1020	20.4 (vacuum)	[33]
Yb^{3+} :LLF	1020	15 (air), 5 (water)	[34]
Yb^{3+} :NaYF ₄	1020	9 (D ₂ O)	[36]
Yb^{3+} :NaYF ₄	1020	42 (vacuum)	[39]
Yb^{3+} :KLaF ₄	1020	8.6 (vacuum)	[41]

Deceleration of a nanocrystal through its internal cooling was proposed in [42]. As may be seen in [43], a RE-doped nanocrystal is a charged particle. The source of its surface charge is the doping gradient. In [42], a Paul trap, which is widely used for localizing charged nanostructures, was used (Figure 14).

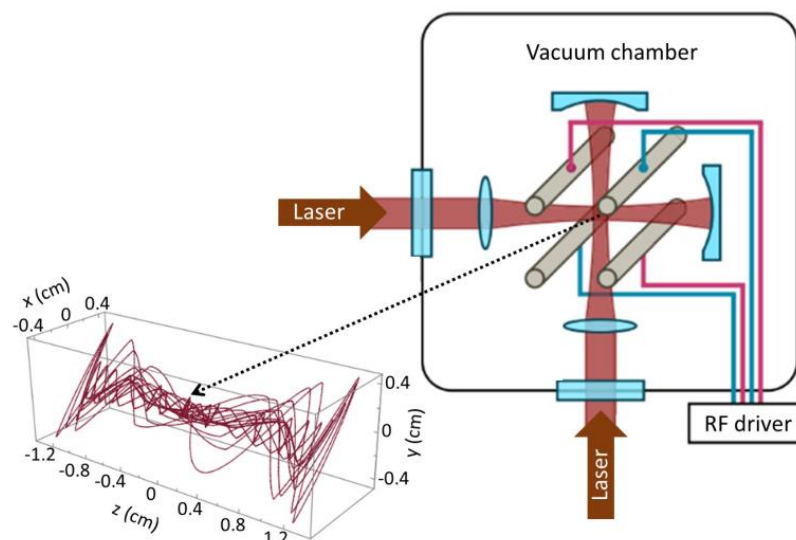


Figure 14. Hybrid trapping and deep laser cooling of a $\text{Yb}^{3+}:\text{CsF}_2$ nanocrystal with the path function of its optical cooling.

The scheme in Figure 14 consists of a Paul trap for nanocrystal spatial localization [40,44] and a 3D standing light wave for the optical cooling of nanocrystals [45]. The standing light wave can be replaced by a single light wave. Indeed, as is evident from the foregoing, RE-doped nanocrystals can be optically cooled with a single optical wave. In the theoretical analysis of optical cooling presented in Figure 14, 5% $\text{Yb}^{3+}:\text{CsF}_2$ nanocrystals were considered. It was assumed that the nanocrystal of mass $M = 6.4 \times 10^{-19} \text{ g}$ was placed in the center of the Paul trap ($x_0 = y_0 = z_0 = 0$) at initial velocities of $v_{0x} = v_{0y} = v_{0z} = 10 \text{ cm} \cdot \text{s}^{-1}$. The nanocrystal dynamics consist of the motions of two kinds: the secular motion and the small oscillations about the secular path (Figure 14). The secular motion takes place along the smooth trajectory, which converge to the center of the Paul trap. The interaction between the charged nanocrystals and radio-frequency field results in small oscillations about the secular path. The numerical simulations presented in [42] prove that the $\text{Yb}^{3+}:\text{CsF}_2$ nanocrystal mechanical action can reach a value $\sim 10\hbar$, which is close to the quantum limit of \hbar .

4. Conclusions

Optical refrigeration based on anti-Stokes fluorescence has dramatically improved over last several years. Early in the development of laser cooling of RE-doped low-phonon solids, *mm*- and *cm*- sized samples were the focus of attention. These bulk samples are interesting for the development of an all-optical solid-state cryocooler, which is free from mechanical vibrations, moving parts, and liquids. The first all-solid-state optical cryocooler started its operation in 2018 [46]. Laser cooling with anti-Stokes fluorescence in bulk samples can also be used for heat mitigation in high-power lasers [47].

At the moment, optical refrigeration of solids has moved to the area of small μm - and *nm*-sized RE-doped low-phonon particles. A hybrid cooling mechanism resulting in a decrease in translational temperature and in internal temperature of the sample has been considered in this paper. The theoretical background of optical refrigeration based on anti-Stokes fluorescence has been presented and discussed. It is shown that Mie resonances can enhance laser cooling in a number of properly designed samples. It has been shown that hybrid trapping can be used for the localization and internal cooling of RE-doped nanocrystals. This approach can be applied to the fundamental studies in biophysics, chemistry, and medicine.

It has been shown that hybrid laser cooling can be realized using a single-beam optical trapping. This approach can be useful for physiological laser refrigeration and for future levitated hybrid opto-mechanics experiments, where the control of translational

and internal temperatures is important. For example, using this approach and Yb³⁺:YLF nanocrystals, one can build a levitated nanocryostat. The birefringence of the particles can be used to control their space orientation. Laser cooling of RE-doped nanocrystals can also be used to mitigate heat generated in spherical microlasers [48].

Laser hybrid cooling of micro- and nanoparticles is in its infancy. I believe that further miniaturization of the RE-doped samples that undergo hybrid laser cooling is in sight. In very small samples (several nm), quantization of phonon modes is very important. As the size of the nanocrystal decreases, its phonon cut-off frequency increases. This effect can deteriorate thermalization in very small particles [27]. Engineering of the host material can be a solution to this problem.

Funding: This research received no external funding.

Institutional Review Board Statement: Not applicable.

Informed Consent Statement: Not applicable.

Data Availability Statement: Not applicable.

Conflicts of Interest: The author declares no conflict of interest.

References

- Fischer, E. Die dreidimensionale Stabilisierung von Ladungsträgern in einer Vierpolfeld. *Z. Phys.* **1959**, *156*, 1–26.
- Dehmelt, H.G. Radiofrequency spectroscopy of stored ions. I. Storage. *Adv. At. Mol. Phys.* **1967**, *3*, 53–72.
- Dehmelt, H.G. Radiofrequency spectroscopy of stored ions. II. Spectroscopy. *Adv. At. Mol. Phys.* **1969**, *5*, 109–154.
- Byrne, J.; Farago, P.S. On the production of polarized electrons by spinexchange collisions. *Proc. Phys. Soc.* **1965**, *86*, 801–815.
- Gräff, G.; Klempt, E.Z. Messung der Zyklotronfrequenz im Vierpolkäfig. *Zeitschrift Für Naturforschung* **1967**, *22*, 1960–1962.
- Sokolov, A.; Pavlenko, Y.G. *Opt. Spectrosc.* **1967**, *22*, 1–3.
- Penning, F.M. Introduction of an axial magnetic field in the discharge between two coaxial cylinders. *Physica* **1936**, *3*, 873–894.
- Letokhov, V.S. Doppler line narrowing in a standing light wave. *Pis. Zh. Eksp. Teor. Fiz.* **1968**, *7*, 348. (In English)
- Hansch, T.W.; Schawlow, A. Cooling of gases by laser radiation. *Opt. Commun.* **1975**, *13*, 68.
- Wineland, D.; Dehmelt, H. Proposed $10^{14} \Delta\nu < \nu$ laser fluorescence spectroscopy on Tl⁺ mono-ion oscillator III. *Bull. Am. Phys. Soc.* **1975**, *20*, 637.
- Lett, P.; Watts, R.; Westbrook, C.; Phillips, W.D.; Gould, P.; Metcalf, H. Observation of atoms laser cooled below the Doppler limit. *Phys. Rev. Lett.* **1988**, *61*, 169–172.
- Anderson, M.H.; Ensher, J.R.; Matthews, M.R.; Wieman, C.E.; Cornell, E.A. Observation of Bose-Einstein Condensation in a Dilute Atomic Vapor. *Science* **1995**, *269*, 198–201.
- Davis, K.B.; Mewes, M.-O.; Andrews, M.R.; van Druten, M.J.; Durfee, D.S.; Kurn, D.M.; Ketterle, W. Bose-Einstein Condensation in a Gas of Sodium Atoms. *Phys. Rev. Lett.* **1995**, *75*, 3969. Erratum in *JETP Lett.* 1968, 7, 272. (In English)
- Pringsheim, P. Zwei Bemerkungen über den Unterschied von Lumineszenz- und Temperaturstrahlung. *Z. Phys.* **1929**, *57*, 739–746.
- Epstein, R.I.; Buchwald, M.I.; Edwards, B.C.; Gosnell, T.R.; Mungan, C.E. Observation of laser-induced fluorescent cooling of a solid. *Nature* **1995**, *377*, 500–502.
- Nemova, G. *Laser Cooling: Fundamental Properties and Application*; Pan Stanford Publishing: Singapore, 2016.
- Luo, X.; Eisaman, M.D.; Gosnell, T. Laser cooling of a solid by 21 K starting from room temperature. *Opt. Lett.* **1998**, *23*, 639–641.
- Gosnell, T.R. Laser cooling of a solid by 65 K starting from room temperature. *Opt. Lett.* **1999**, *24*, 1041–1043.
- Nemova, G. *Field Guide to Laser Cooling Methods*; SPIE Press: Bellingham, WA, USA, 2019.
- Sheik-Bahae, M.; Epstein, R.I. Laser cooling of solids. *Laser Photon. Rev.* **2009**, *3*, 67–84.
- Nemova, G.; Kashyap, R. Laser cooling of solids. *Rep. Prog. Phys.* **2010**, *73*, 1–20.
- Seletskiy, D.V.; Hehlen, M.P.; Epstein, R.I.; Sheik-Bahae, M. Cryogenic optical refrigeration. *Adv. Opt. Photon.* **2012**, *4*, 78–107.
- Hoyt, C.W. Laser Cooling in Thulium-Doped Solids. Ph.D. Thesis, University of New Mexico, Albuquerque, NM, USA, 2003.
- Hasan, Z.; Qiu, Z.; Lynch, J. Laser cooling in materials with high concentration of erbium. *Proc. SPIE* **2011**, *7951*, 1–7.
- Melgaard, S.D.; Albrecht, A.D.; Hehlen, M., P.; Seletskiy, D.V.; Sheik-Bahae, M. Solid-state cryo-cooling using optical refrigeration. *CLEO* **2014**, FTh4D.4. [[CrossRef](#)]
- Soares de Lima Filho, E.; Nemova, G.; Loranger, S.; Kashyap, R. Laser-induced cooling of a Yb:YAG crystal in air at atmospheric pressure. *Opt. Express* **2013**, *21*, 24711–24720.
- Nemova, G.; Kashyap, R. Optimization of optical refrigeration in Yb³⁺:YAG samples. *J. Lumin.* **2015**, *164*, 99–104.
- Mie, G. Beiträge zur Optik trüber Medien, speziell kolloidaler Metallosungen. *Ann. Phys.* **1908**, *330*, 377–445.
- Nemova, G.; Caloz, C. Mie resonance enhancement of laser cooling in rare-earth doped materials. *arXiv* **2021**.
- Pant, A.; Xia, X.; Davis, J.E.; Pauzuskie, P.J. Solid-state laser refrigeration of a composite semiconductor Yb:YLiF₄ optomechanical resonator. *Nat. Commun.* **2020**, *11*, 3235.

31. Melgaard, S.D.; Albrecht, A.R.; Hehlen, M.P.; Sheik-Bahae, M. Solid-state optical refrigeration to sub-100 kelvin regime. *Sci. Rep.* **2016**, *6*, 20380.
32. Rahman, A.A.; Barker, P. Laser refrigeration, alignment and rotation of levitated Yb³⁺: YLF nanocrystals. *Nat. Photonics* **2017**, *11*, 634–638.
33. Dobretsova, E.A.; Xia, X.; Pant, A.; Lim, M.B.; De Siena, M.C.; Boldyrev, K.N.; Molchanova, A.D.; Novikova, N.N.; Klimin, S.A.; Popova, M.N.; et al. Hydrothermal Synthesis of Yb³⁺: LuLiF₄ Microcrystals and Laser Refrigeration of Yb³⁺: LuLiF₄/Silicon-Nitride Composite Nanostructures. *Laser Photonics Rev.* **2021**, *15*, 2100019.
34. Dobretsova, E.A.; Pant, A.; Xia, X.; Garipey, R.E.; Pauzauskie, P.J. Safe and Scalable Polyethylene Glycol-Assisted Hydrothermal Synthesis and Laser Cooling of 10% Yb³⁺: LiLuF₄ Crystals. *Appl. Sci.* **2022**, *12*, 774.
35. Jain, V.; Gieseler, J.; Moritz, C.; Dellago, C.; Quidant, R.; Novotny, L. Direct measurement of photon recoil from a levitated nanoparticle. *Phys. Rev. Lett.* **2016**, *116*, 243601.
36. Zhou, X.; Smith, B.E.; Roder, P.B.; Pauzauskie, P.J. Laser Refrigeration of Ytterbium-Doped Sodium–Yttrium–Fluoride Nanowires. *Adv. Mater.* **2016**, *28*, 8658–8662.
37. Zheng, K.; Qin, W.; Wang, G.; Wei, G.; Zhang, D.; Wang, L.; Kim, R.; Liu, N.; Ding, F.; Xue, X.; et al. Upconversion luminescence properties of Yb³⁺, Gd³⁺ and Tm³⁺ co-doped NaYF₄ microcrystals synthesized by the hydrothermal method. *J. Nanosci. Nanotechnol.* **2010**, *10*, 1920–1923.
38. Roder, P.B.; Smith, B.E.; Zhou, X.; Cranec, M.J.; Pauzauskie, P.J. Laser refrigeration of hydrothermal nanocrystals in physiological media. *Proc. Natl. Acad. Sci. USA* **2015**, *112*, 15024–15029.
39. Luntz-Martin, D.R.; Felsted, R.G.; Dadras, S.; Pauzauskie, P.J.; Vamivakas, A.N. Laser refrigeration of optically levitated sodium yttrium fluoride nanocrystals. *Opt. Lett.* **2021**, *46*, 3797–3800.
40. Nagornykh, P.; Coppock, J.E.; Kane, B. Cooling of levitated graphene nanoplatelets in high vacuum. *Appl. Phys. Lett.* **2015**, *106*, 244102.
41. Xia, X.; Pant, A.; Zhou, X.; Dobretsova, E.A.; Bard, A.B.; Lim, M.B.; Roh, J.Y.D.; Gamelin, D.R.; Pauzauskie, P.J. Hydrothermal synthesis and solid-state laser refrigeration of ytterbium-doped potassium-lutetium-fluoride (KLF) microcrystals. *Chem. Mater.* **2021**, *33*, 4417–4424.
42. Rudyi, S.S.; Vovk, T.A.; Kovalev, A.V.; Polyakov, V.M.; Ivanov, A.V.; Perlin, E.Y.; Rozhdestvensky, Y.V. Deep laser cooling of rare-earth-doped nanocrystals in a radio-frequency trap. *J. Opt. Soc. Am. B* **2017**, *34*, 2441–2445.
43. Diaz-Torres, L.; de la Rosa, E.; Salas, P.; Desirena, H. Enhanced cooperative absorption and upconversion in Yb³⁺-doped YAG nano-phosphors. *Opt. Mater.* **2005**, *27*, 1305–1310.
44. Kuhlicke, A.; Schell, A.W.; Zoll, J.; Benson, O. Nitrogen vacancy center fluorescence from a submicron diamond cluster levitated in a linear quadrupole ion trap. *Appl. Phys. Lett.* **2014**, *105*, 73101.
45. Lett, P.D.; Phillips, W.D.; Rolston, S.; Tanner, C.E.; Watts, R.; Westbrook, C. Optical molasses. *J. Opt. Soc. Am. B* **1989**, *6*, 2084–2107.
46. Hehlen, M.P.; Meng, J.; Albrecht, A.R.; Lee, E.R.; Gragossian, A.; Love, S.P.; Hamilton, C.E.; Epstein, R.I.; Sheik-Bahae, M. First demonstration of an all-solid-state optical cryocooler. *Light: Sci. Appl.* **2018**, *7*, 1–10.
47. Nemova, G. Radiation-balanced lasers: History, status, potential. *Appl. Sci.* **2021**, *11*, 1–23.
48. Xia, X.; Pant, A.; Felsted, R.G.; Garipey, R.E.; Davis, E.J.; Pauzauskie, P.J. Radiation balanced spherical microlaser. *Proc. SPIE* **2021**, *11702*, 1–4.